2011

Performance Comparison of Layered Composite Bimodal Fiber Mats with Unimodal Fiber Mats

Sukhada Sanjay Kulkarni
Virginia Commonwealth University

School of Engineering
Virginia Commonwealth University

This is to certify that the thesis prepared by Sukhada Sanjay Kulkarni entitled PERFORMANCE COMPARISON OF LAYERED COMPOSTIE BIMODAL FIBER MATS WITH UNIMODAL FIBER MATS has been approved by her committee as satisfactory completion of the thesis requirement for the degree of Master of Science in Engineering.

Gary C Tepper, Ph.D., Thesis Director, Chair of Mechanical Engineering, School of Engineering

---

Hooman Vahedi Tafreshi, Ph.D., School of Engineering

Gary L Bowlin, Ph.D., School of Engineering

Russell D. Jamison, Ph.D., Dean, School of Engineering

F. Douglas Boudinot, Ph.D., Dean of Graduate Studies

Date

PERFORMANCE COMPARISON OF LAYERED COMPOSITE BIMODAL FIBER MATS WITH UNIMODAL FIBER MATS

A thesis submitted in partial fulfillment of the requirements for degree of Master of Science at Virginia Commonwealth University

By

SUKHADA SANJAY KULKARNI

Bachelors in Mechanical Engineering, University of Pune, 2005

Director: Dr. Gary. C. Tepper

PROFESSOR, MECHANICAL & NUCLEAR ENGINEERING

Virginia Commonwealth University

Richmond, Virginia

July, 2011

Acknowledgement

I am really fortunate to have so many wonderful people to thank for their help in this thesis. I am deeply grateful to my advisor, Dr. Gary. C. Tepper for giving me the freedom to experiment my ideas. He encouraged and supported me in difficult times. I would have been lost without his mentorship.

A special thanks to Dr. Joan Rosell and Dr. Dmitry Pestov for their guidance and support in my research. I thank Dr. Garry Glaspell for his unending patience and help in drafting this thesis. I am grateful to my committee members Dr. Hooman Tafreshi and Dr. Gary Bowlin for their continual support and encouragement.

I would also like to thank my lab mates- Ken Chen, Ezzat Elshazly, Negar Ghochaghi, Thu Ho for their cooperation. I also thank Kurt Spitzner, Austin Dubose and Gray Lawson for their assistance.

No vocabulary is sufficient enough to express my gratitude to my family. I can only thank them for their love and support throughout my life. Had it not been for them, this research and my coursework would have been impossible.

Table of Contents

List of Tables vi

List of Figures vii

Abstract viii

Chapter

1 Introduction and Theory 1

1.1 Introduction 1

1.2 Electrospinning Theory and Process 5

1.3 Electrospinning Process Parameters 6

1.4 History of Electrospinning 10

1.5 HEPA Filtration Standards 12

1.6 Filter Performance Parameters 13

1.7 Single Fiber Efficiency 17

1.8 Means of Particle Capture 17

1.9 Total Filter Efficiency 25

1.10 Pressure Drop 26

1.11 Aerodynamic Slip 27

1.12 Figure of Merit 29

1.13 Bimodal Filter Media 29

1.14 Purpose of Research Study 31

List of References 32

2 Experimental Setup 42

2.1 Materials 43

2.2 Electrospinning Apparatus 45

2.3 Filter Test Rig 47

2.4 Optical Particle Counter 50

2.5 Scanning Electron Microscope 51

2.6 Optical Microscopy 51

2.7 Weighing Scale 52

2.8 Data Analysis Methods 52

2.9 Neutralization of Surface Charge 53

2.10 Effect of Corona Voltage on Fiber Mat 54

2.11 Bimodal Deposition 55

List of References 58

3 Results and Discussion 59

3.1 Unimodal Filter Mats 59

3.2 Bimodal Filter Mats 61

3.3 Filter Mat Morphology 62

3.4 Comparison of Performance of Unimodal and Bimodal Mats 64

3.5 Theoretical Calculations 67

List of References 72

4 Conclusion 73

List of Tables

1.1 HEPA and ULPA rating system outline 12

2.1 Performance of simultaneous and sequential bimodal mats ..56

3.1 Table of performance of unimodal filters of 0.33 ± 0.01 mg 60

3.2 Table of performance of unimodal filters of 0.66 ± 0.01 mg 60

3.3 Table of performance of bimodal filters of 0.33 ± 0.01 mg ..62

3.4 Table of performance of bimodal filters of 0.66 ± 0.01 mg ..62

3.5 Table for thickness of fiber mats 64

3.6 Table for solidity of filter mats 67

3.7 Table for pressure drop comparison 69

3.8 Table for efficiency comparison 70

3.9 Table for FOM comparison 71

List of Figures

1.1 Taylor Cone 8

1.2 Particle capture by interception 18

1.3 Particle capture by inertial impaction 19

1.4 Particle capture by diffusion 21

2.1 Electrospinning setup.....46

2.2 Filter test rig arrangement.....48

2.3 Filter test rig.....50

2.4 Electric breakdown created holes 55

2.5 Chart depicting efficiency comparison 57

3.1 Histogram depicting the fiber diameter deposition.....63

3.2 SEM Image: Unimodal fiber mats 63

3.3 SEM Image: Bimodal fiber mats 63

3.4 Chart comparison between unimodal and bimodal filters for pressure drop 66

3.5 Chart comparison between unimodal and bimodal filters for efficiency.....66

3.6 Chart comparison between unimodal and bimodal filters for figure of merit.....67

Abstract

PERFORMANCE COMPARISON OF LAYERED COMPOSITE BIMODAL FIBER MATS WITH UNIMODAL FIBER MATS

By Sukhada Sanjay Kulkarni, B.E

A thesis submitted in partial fulfillment of the requirements for degree of Master of Science at Virginia Commonwealth University

Virginia Commonwealth University, 2011

Director: Dr. Gary. C. Tepper, Professor, Mechanical Engineering

This study was conducted to evaluate and compare performance of unimodal and bimodal mats with approximately same mass. 10% and 18% Nylon 4, 6 polymer solution were used for electrospinning the fibers. A negative ion source was used to neutralize the surface charge. The fiber diameters were measured with SEM and were <500 nm thus incorporating the slip effect. Bimodal mats were prepared from different deposition modes. Optimal mode was selected on analyzing the performance factors. The bimodal mats were then compared with unimodal mats. For their performance the fiber mass for these mats was approximately the same. It was observed that the unimodal mats had higher

efficiencies and higher pressure drop giving a lower FOM. Bimodal mats showed lower efficiencies and pressure drop compared to unimodal mats. However, the FOM for bimodal mats was approximately 200% higher than unimodal mats

CHAPTER 1

INTRODUCTION AND THEORY

1.1 Introduction

Nanotechnology is a field which primarily deals with the building of devices and materials at nano scale. As the size decreases from micro or millimeter to nanometer, material properties and characteristics change. This is due to the fact that electrons interact differently depending upon the dimensions and structure of the material. Dimensionality thus plays an important role in determining the material property. 1-D nano structures are typically fibers, wires, rods, belts, tubes, spirals and rings having diameters in the range of 1–100 nm. These structures play a critical role in functionality and integration of nano devices as they are the smallest systems to transport electrons efficiently. These structures provide a good system to study the effect of electrical and thermal transport or mechanical properties on dimension and size reduction. Nanofibers are used in a variety of applications some of

which include tissue engineering, catalytic reaction materials, electrochemical electrodes, affinity membranes, and nano-composites [1 – 3].

One application of nanofibers is filtration. Filters are widely used in home HVAC systems, hospitals or even in manufacturing and processing industry. Filtration is important in these areas as they remove the contaminant particles from air or liquid. High Efficiency Particulate Air (HEPA) filters are the most commonly used commercial air filters for clean air. The need for high efficiency filters arose primarily for the sake of health protection. The typical fibrous filters have the minimum efficiency for the particle sizes in the range of 0.1 micrometer to 0.5 micrometer. Most airborne viruses and bacteria are in the range of 0.2-0.4 micrometers. For example, the mycobacterium tuberculosis is a rod shaped bacterium with a diameter of 0.3-0.6 microns with an average length of 1-4 microns [4]. Respirators operate in two ways- particle removal from supply air and removal of airborne particles produced in vicinity of critical surfaces [5]. Another use of high efficiency filters is to remove radioactive particles. Radioactive materials occur naturally on earth. These materials undergo radioactive decay until a stable non- radioactive element is formed. People working in uranium mining and nuclear industry are exposed daily are in high risk of developing lung and thyroid

cancers and need to be protected from inhaling ionizing radio nuclides. As a result, the nuclear industry requires almost exclusively HEPA and ULPA (ultra low particulate air) filters for working personnel [6–7]. Nanofibrous media properties like low basis weight, high permeability and small pore size make them suitable for filtration applications [8].

A variety of methods can be used to synthesize nanofibers. Conventional commercial methods such as drawing, template synthesis, phase separation, self assembly, and electrospinning are discussed in brief.

Drawing is a method similar to conventional dry spinning. This method produces long single nanofibers one at a time. These fibers can be precisely positioned on a surface during their fabrication. However, the process requires a viscoelastic material which can sustain strong deformations but is also cohesive enough to support the stresses while pulling [9]. Template synthesis utilizes synthesizing the desired material within the pores of a nanoporous membrane. The membranes employed have cylindrical pores of uniform diameter. The end result is a nanoporous membrane used as a template to make nanofibers of solid or hollow shape. The materials used however should be electronically conductive [10]. Phase separation involves thermally induced gelation, solvent exchange, and freeze-drying resulting in nano porous foam. The

process is time consuming to produce nano porous foam from solid polymer [11].Self assembly is an automatic process wherein individual components organize themselves in desired patterns and structures. This process too is time consuming to produce long continuous nanofibers [12].

Electrospinning is a technique where fibers are drawn due to the electrostatic force instead of mechanical shear forces. An electric field is applied to the polymer solution. When the surface tension of the polymer droplet is overcome by the electrostatic force, thin fibers are generated which are then collected on a surface of neutral or opposite charge [13]. This process is later described in detail. The electrospun fibers have a very large surface area to volume ratio, flexibilities in surface functionalities, superior mechanical properties like stiffness and tensile strength [8]. Electrospun fibers can be used in a variety of applications such as optical fibers, drug delivery systems, tissue engineering scaffolds, catalytic reaction materials, protective textiles etc. [14, 15].They also have good pore interconnectivity and are capable enough to incorporate active chemistry or functionality on nanoscale level. These properties make them suitable for filtration applications [8]. Electrospun fiber mats have small fiber diameters and large surface areas. This helps in achieving high filtration efficiency even if there is a small decrease in air permeability [16]. Usually the

electrospun fiber mats are deposited on fabric substrates to combine advantages of both materials. The substrate also acts as a support for the spun fibers [16]. Electrospinning gives control over the diameter size of nanofibers. Typically, electrospun nanofibers have diameters in the range of 3nm–1 micron. These diameters are 5–10 times smaller than the smallest fibers produced by melt blowing. It is also the only technique which can produce continuous fibers (high aspect (l/d) ratio). Compared to other conventional techniques, it is also relatively cheaper in fabricating fibers [3, 8, 14].

1.2 Electrospinning theory and process

In electrospinning a strong electric field is applied to draw fibers using the electrostatic force between surface charges. A syringe is filled with the polymer solution and a high voltage is applied to the needle tip. Due to it, charged polymer ions move towards charge of opposite polarity. The interaction between the electrostatic repulsion between polymer ions and the external Columbic force causes the pendant droplet to deform into a conical structure called the Taylor cone and a critical voltage is reached. When the applied voltage is higher than the critical voltage, the repulsive electrostatic force is strong enough to overcome the surface tension of the droplet at the tip of the needle and a fine charged jet is

ejected from the tip of the Taylor cone. The electrostatic repulsions between surface charges cause the fluid to accelerate and stretch the jet. This results in reducing diameter of the jet and the length increases such that a constant amount of mass per unit time passes any point on the axis. The distance between the syringe and the collector is predetermined. Because of low mobilities of charge carriers in organic solvents and polymers, the charge is can move through the liquid for larger distances only if given enough time. After the initiation from the cone, the jet undergoes bending instability and is field directed towards the oppositely charged collector, which collects the charged fibers. As the jet travels through the atmosphere, the solvent evaporates, leaving behind a dry fiber on the collecting device. For low viscosity solutions, the jet breaks up into droplets, while for high viscosity solutions it travels to the collector as fibers. Non woven mats are formed as a result of deposition of continuous fibers [13–21].

1.3 Electrospinning process parameters

Many parameters can affect the electrospinning process and the resultant nanofibers. These parameters can be further classified individually [14]

1.3.1 Solution parameters: viscosity, conductivity, surface tension, elasticity and solution concentration

1.3.2 Governing parameters: hydrostatic pressure in syringe, electric potential, distance between needle tip and collector drum

1.3.3 Ambient parameters: solution temperature, humidity and air velocity

The fiber formation from a droplet can be divided further in three stages- jet initiation and its extension along a straight line, whipping instability and jet solidification [14, 16, 35]

1.3.4 Jet initiation

In 1969, Taylor studied the shape of the polymer droplet produced at the tip of the needle on applying an electric field and found that with the increase in needle potential, the fluid meniscus becomes conical. This jet ejection is due to maximum instability of the liquid surface induced by electric field. By examining fluids of varying viscosity, Taylor determined that an angle of 49.3 degrees is required to balance the surface tension of the polymer with the electrostatic forces. This conical shape of the jet was later referred to by other researchers as the "Taylor Cone" in subsequent literature. The conical shape of the jet is important because it defines the onset of the extensional velocity gradients in the fiber forming process.

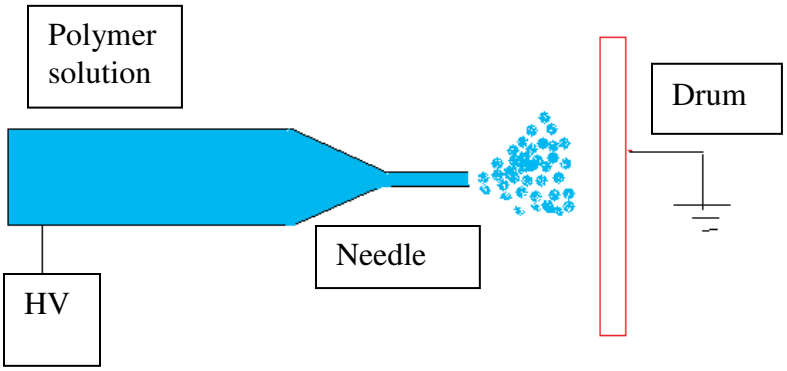

Fig 1.1 Taylor Cone

Another parameter for jet initiation is the strength of the electrostatic field. According to Taylor, maximum instability of jet is developed at the critical voltage Vc (kV). It is given as

$$V_c^2 = 4\frac{H^2}{L^2}\left(\ln\frac{2L}{R} - 1.5\right)(0.117\pi R\gamma) \quad \ldots\ldots\ldots\ldots\ldots\ldots\ldots\ldots\ldots\ldots\ldots\ldots\text{(i)}$$

H is the gap between capillary tip and collector, L is the length of capillary tube, R is the radius of the tube and γ is the surface tension of the fluid. Hendricks et.al; calculated the minimum spraying potential as

$$V = 300 * \sqrt{20\pi r\gamma} \quad \ldots\ldots\ldots\ldots\ldots\ldots\ldots\ldots\ldots\ldots\ldots\ldots\ldots\ldots\ldots\ldots\text{(ii)}$$

Where r is the jet radius.

1.3.5 Jet instabilities

Fluid instabilities occur in this stage. The references predict three types of instabilities for an electrically driven jet.

1) Rayleigh instability: If the applied external electrostatic field is less than the critical value, the jet breaks up into droplets. This phenomenon is called Rayleigh instability and is axisymmetric to jet centerline.

2) Electric field induced instability: This instability too is axisymmetric and causes bead formation

3) Whipping instability: This is a non axisymmetric instability caused mainly due to bending force. If all other process parameters are kept unchanged, the electric field strength is proportional to the instability level. Thus bending occurs when the electric field is at its maximum.

1.3.6 Jet Solidification

As the jet travels along its trajectory for some distance, the solvent is evaporated. If there is sufficient gap between capillary tip and collector the fibers are dried and solidified as they deposit on the drum. If the electrostatic field is high, there is more whipping instability in the jet and this allows for more time for the solvent to

evaporate. The time for solidification changes with the solution concentration and solvent volatability.

1.4 History of Electrospinning

The fundamental principles for electrospraying and electrospinning were established more than 100 years ago. In 1745, Bose documented the jet formation due to electrical forces [22]. This was further studied by Lord Rayleigh who described the various process parameters influencing the jets [23]. Zeleny studied the overcoming of surface tension of a droplet by surface charging leading to the formation of jet and Coulomb expansion. The actual electrospinning process starts with Formhals. He patented [24–28] his experimental process and setup apparatus by which he produced polymer filaments with the help of electric charges. In his first patent, Formhals spun cellulose acetate fibers with acetone as the solvent. The collector was a movable thread collecting device to collect the threads in a stretched condition like that used in conventional spinning. However, due to the short distance between the spinning and collector, the fibers did not dry completely. Vonnegut and Neubauer [29] produced electrified jets of uniform droplets having a size of about 0.1 mm in diameter in 1952. The apparatus used was a small glass capillary. It was filled with water and an electric wire was put in it. In 1955, Drozin [30] used a similar apparatus and researched the dispersion of liquids into

aerosols under high electric potentials. He found that under proper conditions, the aerosol had droplets of relatively uniform size. He also captured different stages of the dispersion. Simons patented an apparatus for producing light weight non-woven fabrics of extremely small diameters. A belt was used as a collector. He observed that the fibers from low viscosity solutions were shorter and finer while more viscous solutions gave relatively continuous fibers[31]. In 1971 Baumgarten electrospun acrylic fibers with diameters ranging from 0.05-1.1 microns [32]. In 1987, Hayati et al. [33] studied the factors affecting the fiber stability and atomization. They found that when applied voltage was increased, fluids of high conductivity produced highly unstable jets that whipped around in different directions. These unstable jets produced fibers of broad diameter distribution.

From 1993 onwards more research began on nanofibers. The process which earlier was known as electrostatic spinning was coined as electrospinning by Renekar and Doshi of Akron University [34]. In the past 20 years research has been done on experimental and theoretical issues related with electrospun fibers.

1.5 HEPA Filtration Standards

The US Department of Energy defines HEPA filters to have a minimum efficiency of 99.97% at the most penetrating particle size (MPPS) of 300 nm [36]. Other qualities of HEPA filters include low resistance to air flow, reasonable size, sufficient capacity and durability. Generally, these filters are made of mats of fine fibers. The fine fibers provide high collection efficiency. Filtration theory implies that filter fibers must have diameters that are approximately the same as the aerosol particles to be removed [37]. Therefore, the standard HEPA filter medium must have fiber diameters of 0.2 to 0.5 μm to remove sub micrometer particles, and even smaller fiber diameters are necessary for the ultra low particulate air (ULPA) filter medium [38].

The specification used is EN 1822:2009. It defines different classes of HEPA and ULPA at its MPPS of 300 nm. The following table gives the details [36]:

Table 1.1 HEPA and ULPA rating system outline

HEPA Class	Retention (total)	Retention (Local)
E10	>85%	-
E11	>95%	-
E12	>99.5%	-
H13	>99.95%	>99.75%
H14	>99.995%	>99.975%
U15	>99.9995%	>99.9975%
U16	>99.99995%	>99.99975%
U17	>99.999995%	>99.9999%

1.6 Filter performance parameters

The performance of a filter depends on major factors like solid volume fraction, fiber diameter, thickness, face velocity and fiber orientation.

1.6.1 Fiber diameter

This is the most important parameter since it relates directly to interception and impaction modes of aerosol capture. Smaller fibers contribute to interception efficiency while larger fibers help impaction capture. Generally, the fibers in a filter would not be monodispersed; i.e. they would not have exactly the same size. The fiber diameters usually fall in a range for a given set of parameters. The thinner fibers exhibit chain entanglement. It has also been proved that the most penetrating particle size decreases with decreasing fiber diameter. Thus efficiency increases with ultrafine fibers [38–39]

1.6.2 Solid Volume fraction

It is also called as solidity (α). For any given filter, it is defined as the ratio of actual mass of solid material to the total volume of fiber. As solidity increases, the resistance to flow also increases. The efficiency of a filter also increases with increasing SVF.

Normally for fibrous air filters the SVF is in a range of 0.001 -0.02 typically 0.01 [40–41].

$$\alpha = \frac{W}{\rho t} \quad \text{.....} \quad (1)$$

Where W is the basis weight of the filter, ρ is density of fiber and t is the thickness of the filter [38, 42].

Kuwabara hydrodynamic factor [53–55] deals with flow around the fiber and is dependent only on the solid volume fraction. It is given by

$$Ku = -0.5\ln\alpha - 0.75 + \alpha - 0.25\alpha^2 \quad \text{.....} \quad (2)$$

Solid volume fraction is an important parameter for filter efficiency since it is closely related to the individual streamlines for a fiber.

1.6.3 Thickness of filter mat

A filter mat can contain any number of layers. The total thickness of the mat is the thickness of all the layers of fibers constituting the filter. If the substrate contributes to the filtration, only then its

thickness would be considered in the mat thickness. Witzmann [44] established that the penetration through the filter decreases exponentially with filter thickness.

If the filter efficiency is E then

$$E = 1 - EXP(-k/t) \quad \ldots\ldots\ldots\ldots\ldots\ldots\ldots\ldots\ldots\ldots (5)$$

Where k is the constant for filtration and t is the mat thickness. It is quite possible that the top layers would capture more particles compared to bottom layers. However, the probability of capturing a particle increases with increasing number of layers. However, as the thickness increases the pressure drop across the filter also increases.

1.6.4 Face Velocity

The efficiency is proportional to the face velocity. For an uncharged filter mat, the efficiency increases with increasing face velocity. This is largely due to effect of velocity on the capture mechanisms.

1.6.5 Fiber Orientation [42]

The structure of fibrous mats can be classified in three ways [43–47]

1) Unidirectional structures (axes of all fibers parallel to each other)

2) random layered planar structures where axes of fibers are mostly perpendicular to the flow direction

3) 3-D isotropic structures where fiber axes can be randomly orientated in space

Most non woven mats fall in category (2) and (3). Banks *et. al* [48–49] developed single fiber model to study effects of through plane fiber orientation on pressure drop and efficiency due to diffusion. Schweers and Loffler [50] developed an expression for the relation between through fiber orientation and single fiber efficiency for interception. None of these models have been tested experimentally. Fotovati and Tafreshi [51] were the first to predict the effect of in-plane fiber orientation and through-plane fiber orientation on filter performance with respect to fiber diameter. They predicted that for nano fibers, as the relative size between particle diameter and fiber diameter is large, in-plane orientation plays an important role in collection efficiency. The filtration efficiency of a nanofiber filter can be increased by decreasing the in-plane fiber orientation. Through- plane orientation does not play a role in case of nanofibers. Pressure drop is not affected by either plane fiber orientation [42, 44, 47, 52].

1.7 Single Fiber Efficiency

Theoretically, efficiency of fibrous filtration is calculated by isolating a single fiber with its axis positioned perpendicular to the airflow. Effects of different capture mechanisms for that fiber are then studied.

If the flow around a fiber is distorted, the flow around its neighboring fibers is also affected. The modern single fiber theory considers the effect of neighboring fibers using Kuwabara's cell model theory [53–54].

1.8 Means of Particle Capture

There are three major modes of capture: direct interception, inertial impaction and diffusion deposition. Capture mechanisms like gravitational settling and electrostatic attraction between the particles and the fibers also contribute in particle capture. These different mechanisms are discussed in detail below:

1.8.1 Direct Interception

If a particle following a gas streamline approaches a fiber within one particle radius, it sticks to the fiber and gets captured. The airflow pattern in Stokes flow is independent of velocity. Hence interception too is independent of air velocity. It does not depend on the viscosity of air as the particles do not move relative to air. At low air densities, high efficiency at low pressures is observed

for very fine fibers. Particle size is critical in interception. Single fiber efficiency due to interception increases with increase in particle diameter. Direct Interception is most efficient for particle sizes above 400 nm [38, 55].

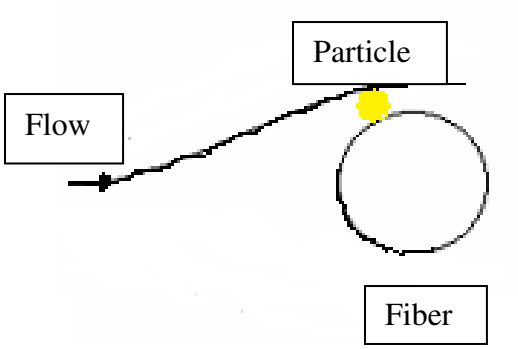

Fig 1.2 Particle Capture due to interception

The single fiber efficiency due to interception depends on the dimensionless parameter N_R where

$$N_R = \frac{d_p}{d_f} \quad \ldots\ldots. (4)$$

d_p and d_f are the particle and fiber sizes respectively

Liu and Liu and Rubow (1990) [20] gave the expression for single fiber efficiency for interception, E_R

$$E_R = 0.6\left(\frac{1-\alpha}{Ku}\right)\left(1+\frac{Kn}{R}\right)\left(\frac{R^2}{1+R}\right).....(5)$$

1.8.2 Inertial Impaction

As the name suggests, this capture mode occurs because of the particle's inertia. A particle entering the flow field surrounding the fibers must follow the curved path of the streamlines so it can pass around the obstacle. Streamlines try to move away as they come closer to the fiber. Particles of heavy mass possess sufficient inertia and are unable to change their path fast enough to adjust to the abruptly changing streamlines near the fiber. They cross the streamlines to hit the fiber and get captured. Single fiber efficiency for inertial impaction increases with the velocity of the air approaching the fiber and increase in Stokes number. Inertial impaction is observed generally for particles above 600 nm [38, 55].

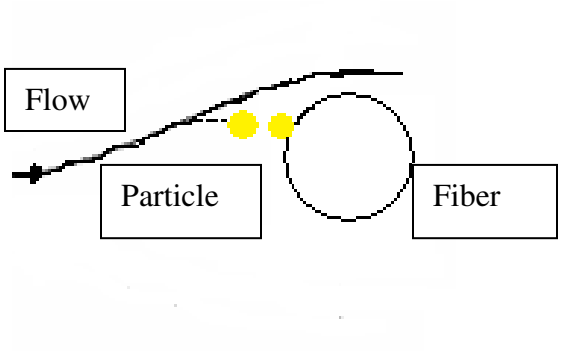

Fig 1.3 Particle capture due to inertial impaction

$$\text{Stokes number} = Stk = \frac{\rho^2 d_p{}^2 C_c V}{18\mu d_f} \text{.....(6)}$$

Stechkina, Kirsh & Fuch (1969) [56–57] gave the expression for single fiber efficiency due to inertial impaction

$$E_I = \frac{(Stk)J}{(2Ku)^2} \text{.....(7)}$$

$$\text{Where } J = (29.6 - 28\alpha^{0.62})R^2 - 27.5R^{2.8} \text{ .....(8)}$$

1.8.3 Diffusion

When suspended particles are very small they closely follow the streamlines. However, they are in Brownian motion. At thermal energy equilibrium every gas molecule has energy of $0.5k_bT$ where k_b is Boltzmann constant. Particles in contact with these gas molecules are also in equilibrium. The constant exchange of energy between molecule and particles causes Brownian motion. Particle may collide when moving randomly. The velocity of the particle is decreased after collision. When the particle gets closer to the fiber, it gets captured. Particle sizes till 50 nm- 200 nm are mostly captured by diffusion.

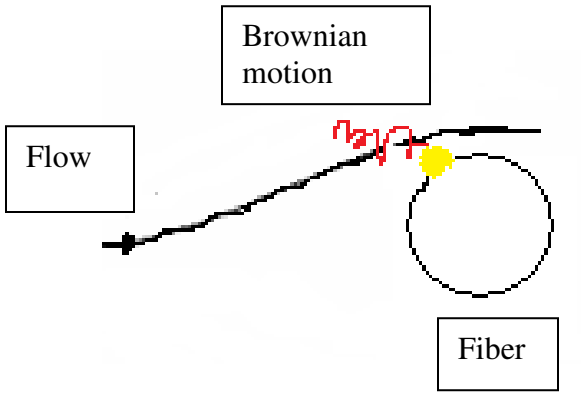

Fig 1.4 Particle capture due to diffusion

The single fiber efficiency due to diffusion depends mainly on Peclet number where Peclet number Pe,

$$Pe = \frac{Vd_f}{D} \text{.....(9)}$$

V is the velocity and D is the particle diffusion coefficient.

$$\text{Diffusivity } D = \frac{k_b C_c T}{3\pi\mu d_p} \text{.....(10)}$$

k_b is Boltzmann Constant = $1.38 * 10^{-23}\ m^2 kg s^{-1} K^{-1}$

T: absolute air temperature

μ: air viscosity

C_c: Cunnigham Factor

$$C_c = 1 + K_n \left[1.207 + 0.44 \exp\left(\frac{-0.78}{K_n} \right) \right] \quad \ldots\ldots\ldots\ldots (11)$$

The single fiber efficiency for diffusion is $E_D = 2.7 Pe^{\frac{-2}{3}}$ …… (12)

The single fiber efficiency for diffusion increase with increase in Peclet number and decrease in particle size. Diffusion is the only deposition mechanism whose single fiber efficiency increases with decrease in particle size.

The expression for single fiber efficiency considering the aerodynamic slip effect is given by Pich [58–60]

$$E_D = 2.27 Ku^{-1/3} Pe^{-2/3} (1 + 0.62 KnPe^{1/3} Ku^{-1/3}) \ldots\ldots\ldots (13)$$

1.8.4 Gravitational settling

Aerosol particles in still air tend to settle out under the influence of gravity. The same principle applies for particles suspended in the air are flowing through a filter. The particle comes in contact with the fiber through gravitational deposition. The effect of gravity during filtration depends on the direction of airflow. Settling velocity will capture the particle while the convective velocity will

carry the particles past through the fibers. The efficiency depends on the relative sizes of the two.

The single fiber efficiency due to gravitational settling is given by Brown (1993) [38]

$$E_G = \frac{d_p{}^2 \rho g}{18 \eta V} \text{.....(14)}$$

1.8.5 **Electrostatic Attraction** [38]

This mechanism is mostly ignored because of the difficulty in quantifying the charge on particles and the fibers. Both charged and neutral particles are attracted to electrically charged fibers. Charged particles are attracted to oppositely charged fibers by Columbic forces. The strength of induced dipole depends on the volume of the particle and the dielectric constant of its material. Like in gravitational settling, the efficiency of an electrostatic filter depends on the ratio of the drift and convective velocities. For an electrically charged filter, the collection efficiency increases with decreasing face velocity. The efficiency also increases with increasing the charge on the fibers or the particles.

The electric field at a distance from a filter fiber carrying uniform chare Q per unit length acts purely in the radial direction and has a magnitude E given by

$$E = \frac{Q}{2\pi\varepsilon_0 r} \quad \ldots\ldots\ldots (15)$$

E is the permittivity of free space

If the particle has a diameter d_p and a charge q, the drift velocity is given by the product of force acting on it and its mechanical mobility μ

$$V_d = \frac{QqC_n}{6\pi^2\varepsilon_0 d_p r} \ldots\ldots (16)$$

The electrical mobility of a particle μe is given by

$$\mu_e = \frac{V_d}{E} \ldots\ldots (17)$$

$$\mu_e = \frac{q}{3\pi\eta d_p} \ldots\ldots (18)$$

The quotient of drift velocity and convective velocity gives the dimensionless parameter for single fiber efficiency for capture by permanently charged fibers

$$N_{Qq} = \frac{Qq}{3\pi^2 \eta d_p d_f U} \text{.....(19)}$$

The single fiber efficiency will be evaluated at a fixed distance from fiber axis since the drift velocity depends on the distance.

For a neutral fiber and a charged particle with charge q, Brown [38] gives the single fiber efficiency as

$$E_q = 1.5\left[\frac{(\varepsilon f - 1)q^2}{(\varepsilon f + 1)12\pi^2 U_0 \varepsilon_0 d_p d_f{}^2}\right]^{1/2} \text{.....(20)}$$

ε_f is the relative permittivity of the fiber material

1.9 Total Filter Efficiency [14]

The single fiber efficiencies for each capture mechanism are calculated with the assumption that each mechanism is acting independently. Combining these efficiencies would give the total single fiber efficiency.

The single fiber efficiency is given by

$$E = 1 - (1 - E_D)(1 - E_R)(1 - E_I)(1 - E_G) \text{.....(21)}$$

E_D, E_R and E_I are the single fiber efficiencies due to diffusion, interception and inertial impaction respectively [55, 61–63].

For any filter, its total efficiency is given by η

$$\eta = 1 - P \ldots\ldots. (22)$$

Where P is the penetration of air particles through the filter and Δ p is the pressure drop across the filter.

$$P = \frac{\text{particle concentration downstream of the filter}}{\text{particle concentration upstream of the filter}} \quad \ldots..(23)$$

Payet *et.al* correlation (1992) [38, 55, 64] gives the efficiency of filters under slip flow conditions.

$$\eta = 1 - \exp\left[-\frac{4\alpha E t}{\Pi(1-\alpha) d_f} \right] \qquad \ldots\ldots(24)$$

Where the thickness of the filter is t and d_f is the diameter of fiber

Often, one mechanism is predominant in capturing particles and the overall efficiency can be assumed to depend only on that mechanism.

The theoretical efficiency is often overestimated using these expressions as the actual streamlines might differ in reality.

1.10 Pressure Drop

In a fibrous filter, the pressure drop or resistance to the flow across the filter is due to the combined effect of each fiber resisting the flow through it. The pressure drop is actually the total drag force of

all the fibers. According to Rao and Faghri (1988) [65], the pressure drop for the filter is dependent on air viscosity, fiber diameter, filter thickness, face velocity and dimensionless pressure drop *f (α)*

$$\Delta p = f(\alpha)\frac{\mu t V}{d^2_f} \quad \text{……..} \quad (25)$$

Dimensionless pressure drop is calculated from Davies's correlation (1973) [66]

$$f(\alpha) = 64\alpha^{3/2}(1+56\alpha^3) \text{.....} (26)$$

1.11Aerodynamic Slip

In fluid dynamics, the no slip condition pertains to the fact that at a solid boundary the fluid velocity is zero relative to the boundary. This effect is true for air filters whose fibers are in 10 micron size and above. However for nanofibers (fiber sizes less than 500 nm), the classic continuum approach is no longer valid. As fiber diameters are close to the mean free path (66 nm at STP) the molecular movements of air molecules are significant in relation to the size of the fibers and flow field. The drag force acting on a fiber is considerably reduced and hence smaller pressure drop is

measured across the filter [44, 54, 67].The aerodynamic slip factor depends on Knudsen Number given by

$$Kn = 2\lambda / d_f \quad \ldots\ldots..(27)$$

λ and d_f are the mean free path of air and fiber diameter respectively

There are four different flow regimes around a fiber. The flow regimes depend on the fiber diameter and the thermal conditions of the gas. Continuum flow exists for Kn <0.001, slip flow is present for Kn between 0.001 to 0.25, transition regime for 0.25< Kn <10 and free molecule regime prevails for Kn>10. Most nanofibers are typically less than 500 nm and hence air flow is in slip flow regime [64, 67–69].

Maze *et. al* (2007) [70] proposed that the streamlines get closer to the fiber surface with increase in slip velocity. This means that the greater the slip velocity, the lesser the influence of the fibers on the flow field. It was also observed experimentally that permeability of a nanofiber medium should be greater than previously calculated by Jackson and James (1986) [13] and Spielman and Goren (1968) [26]. Hosseini and Tafreshi (2010) [68–69] introduced a correction factor for all expressions involving permeability to incorporate for the slip effect. The correction factor C_r is the ratio of pressure drop under slip flow to pressure drop under no slip flow.

$$C_r = \frac{\Delta p_{ns}}{\Delta p_s} \quad \text{……..(28)}$$

$$where \Delta p_{ns} = \frac{4\mu\alpha t V}{r^2 Ku} \quad \text{……..…….(29)}$$

$$and \Delta p_s = \frac{4\mu\alpha t V(1+1.996Kn)}{r^2(Ku+1.996Kn(-0.5\ln\alpha - 0.25 + 0.25\alpha^2))} \quad \text{……..(30)}$$

1.12 Figure of merit or Quality Factor

The overall performance of a filter depends on both its efficiency as well as its resistance to flow. Pressure drop is related to energy expenditure. Hence the quotient of the logarithm of the penetration and the pressure drop is a measure of performance achieved against energy expended.

FOM or QF is denoted as Q and is given by

$$Q = \frac{-\ln(P)}{\triangle p} \text{.....(31)}$$

The Department of Energy states that The FOM for HEPA filters at MPPS of 0.3 micrometers should be 0.04.

1.13 Bimodal filter media

Most fibrous media research has been done where only one fiber diameter distribution is considered, hence forth referred as unimodal medium in the thesis. These fiber diameters are usually

very small and provide high filtration efficiency. However, these fine fibers lack mechanical rigidity. They also contribute to the large pressure drop for HEPA filters for MPPS of 0.3 μm. Fibrous filters however can also be a binary blend of fine and coarse fibers with two different average diameters. The fine fibers would be highly efficient in particle capture while the coarse fibers would mechanically strengthen the filter.

Brown (1993) proposed that by mixing two different particle sizes, the value for pressure drop for a bimodal filter is close to that across a filter made of unimodal filters. The unimodal fiber diameter is equal to the arithmetic mean of those fibers in question, provided the ratio sizes is less than 2-3. If the ratio is greater the pressure drop is smaller than calculated from the mean size.

There are no simple expressions used to predict collection efficiencies and pressure drop for bimodal media. The simplest way to make a theoretical model is to use an unimodal equivalent diameter which can be substituted in the existing theoretical equations.

Brown and Thorpe [72] indicated that the pressure drop of bimodal fibers is similar to that of unimodal fibers with the same SVF and fiber arrangement but with an unimodal equivalent diameter given by area weighted average of the fine and coarse fibers. Tafreshi *et. al* (2009) found that the error percentage was sensitive to the ratio

of coarse and fine fibers. They proposed a solution where the equivalent diameter is the cube root of weighted mean cube of fiber diameters.

$$d^{cr}_{eq} = 2 * \sqrt[3]{n_c r_c^{\ 3} + n_f r_f^{\ 3}} \quad \text{……..(32)}$$

n_c, n_f, r_c, r_f are the number fractions and radii of coarse and fine fibers respectively [57, 64, 68, 69, 73, 74].

1.14 Purpose of research study

Electrospinning produces very thin, continuous nanofibers which may be aligned or non- aligned. These nanofibers mats have small surface to volume ratio and the pore size can be controlled in the electrospinning process. This study deals with the performance of non woven non- aligned electrospun mats as air filters. Monodisperse filters (henceforth called unimodals) were prepared from a low 10% weight concentration of Nylon 6 fibers. Polydisperse filters (henceforth called bimodals) were made using 10% and 18% weight concentrations. The bimodal filters were a combination of fine and coarse fibers. The purpose of the study was to compare the performance of unimodal mats and bimodal mats for approximately equal mass. The fiber sizes for the study were <500 nm, thus applicable for the slip effect. The future chapters describe the actual experimental setup and the results for this study.

List of References

1) Hu.J, Odom T.W, Lieber C.M., Chemistry and Physics in One Dimension: Synthesis and Properties of Nanowires and Nanotubes, Acc. Chem.Res., 32 (5),1999, pp 435–445
2) Xia, Y.; Yang, P.; Sun, Y.; Wu, Y.; Mayers, B.; Gates, B.; Yin, Y.; Kim, F. and Yan, H., One-Dimensional Nanostructures: Synthesis, Characterization, and Applications, Advanced materials, 15 (5),2003, pp 353–389
3) D. Li, Y Xia, Electrospinning of nanofibers :reinventing the wheel? , Advanced. Materials,16 (14), 2003, pp 1151–1170
4) Curtis L.T. Prevention of hospital-acquired infections: review of non-pharmacological interventions Journal of Hospital Infections ,69 (3), 2008 , pp 204–219
5) Boni. A, Filter media: Improving filter media to achieve cleaner air Elsevier Filtration and Separation, 45 (9) 2208, pp 20–23
6) J. Wang, O. Meisenberg, Y. Chen, E. Karg, J. Tschiersch, Filtration approach to mitigate indoor thoron progeny concentration, Nukleonika, 55(4), 2010 pp 445 –450

7) Y. Yasuoka, T. Ishikawa, S. Tokonami, H. Takahashi, A. Sorimachi, M. Shinogi, Radon mitigation using an air cleaner, Journal of radio analytical and nuclear chemistry, 279 (3), 2009, pp 885–891

8) R.S. Barhate, S. Ramkrishna, Nanofibrous filtering media: Filtration problems and solutions from tiny materials, Journal of Membrane. Science, 296 ,2007 pp 1–8

9) T. Ondarcuhu and C. Joachim, Drawing a single nanofibre over hundreds of microns. Europhys Lett., 42 (2),1998, pp. 215–220

10) C.R. Martin, Membrane-based synthesis of nanomaterials. Chem. Mater. 8 ,1996, pp. 1739–1746

11) P.X. Ma and R. Zhang, Synthetic nano-scale fibrous extracellular matrix. J Biomed Mat Res. 46 ,1999, pp. 60–72

12) G.M. Whitesides and B. Grzybowski, Self-assembly at all scales. Science 295, 2002, pp. 2418–2421

13) H. Fong and D.H. Reneker, Electrospinning and formation of nanofibers. In: D.R. Salem, Editor, Structure formation in polymeric fibers, Hanser, Munich (2001), pp. 225–246

14) Z.M.Huang, Y.Z.Zhang, M.Kotaki, S.Ramakrishna, Composite Science Technology. 2003, 63, 2223.

15) N. Vitchuli et.al, Electrospun Ultrathin Nylon Fibers for Protective Applications, Journal of Applied Polymer Science, 2010, 116 (4), pp 2181–2187

16) T. Subbiah et.al, Electrospinning of Nanofibers, Journal of Applied Polymer Science, 96, 2005, pp 557–569

17) M. Deitzel, J. Kleinmeyer, J.K. Hirvonen and T.N.C. Beck, Controlled deposition of electrospun poly(ethylene oxide) fibers. Polymer 42 (2001), pp. 8163–8170

18) Ojha S, Afsari. M, Kotek R, Gorga R.E., Morphology of Electrospun Nylon 6 Nanofibers as a function of molecular weight and processing parameters, Journal of App Poly. Sci, 108, 2008, 308–319

19) K Yoon et. al , Functional nanofibers for environmental applications, J. Mater. Chem., 2008, 18, 5326–5334

20) V. Thavasi, Electrospun nanofibers in energy and environmental applications, Energy Environ. Sci., 1, 2008, 205–221

21) D.H. Renekar, I. Chun, Nanometre diameter fibres of polymer, produced by electrospinning, Nanotechnology 7,1996, 216–223

22) Bose G.M, Recheres sur la cause et sur la varitable theorie del'electricite, Wittenberg 1745

23) Raleigh, L. London, Edinburgh and Dublin Phil. Mag J 1882, 44, 184-186

24) Formhals A. US patent 1,975,504, 1934

25) Formhals A. US patent 2,160,962, 1939

26) Formhals A. US patent, 2,187,306, 1940

27) Formhals A. US patent, 2,323,025, 1943

28) Formhals A. US patent, 2,349,950, 1944

29) Vonnegut and R.L. Neubauer. J. of Colloid Science **7** (1952), p. 616

30) V.G. Drozin. J. of Colloid Science 10 (1955), p. 158

31) Simons HL. US patent 3,280,229, 1966.

32) P.K. Baumgarten, Electrostatic spinning of acrylic microfibers. *J.* of Colloid and Interface Science 36 (1971), pp. 71–79

33) Hayati, I.; Bailey, A. I.; Tadros, T. F. Journal of Colloid and Interface Science 1987, 117, 205.

34) J. Doshi, D. H. Reneker, J. Electrost. 1995, 35, 151

35) Reneker, D. H.; Yarin, A. L.; Fong, H.; Koombhongse, S. J. of Applied Physics 2000, 87, 4531

36) D. Sinclair, Penetration of HEPA filters by submicron aerosols, Journal of Aerosol Science **1** (1970), pp. 53–67

37) Kim G.T, Ahn Y.C, Lee J.K, Characteristics of Nylon 6 nanofilter for removing ultra fine particles, Korean Journal of Chemical Engineering, 25 (2), 2008, 368–372

38) Thomas D, Contal P, Renaudin V, Penicot P, Lecrec L, Vendel J Modeling pressure drop in HEPA filters during dynamic filtration, Journal of aerosol science 30 (2), 1999, pp 235–246

39) Brown R.C; Air Filtration an integrated approach to theory and application of fibrous filters, Pergamon Press, Oxford 1993

40) Podgórski A, Application of nanofibers to improve the filtration efficiency of the most penetrating aerosol particles in fibrous filters, Chemical Engineering Science 61,2006, pp 6804 – 6815

41) H.V. Tafreshi, M.S. Rahman, S. Jaganathan, Q. Wang and B. Pourdeyhimi, Analytical expressions for predicting permeability of bimodal fibrous porous media, Chemical Engineering Science 64 (6) (2009), pp. 1154–1159

42) S.A. Hosseini and H.V. Tafreshi, Modeling permeability of 3-D nanofiber media: effects of slip flow, Chemical Engineering Science 65 (2010), p. 2249

43) Hosseini, S.A. and Tafreshi, H.V. (2010). Modeling permeability of porous media made of nanofibers with different three-dimensional fiber orientations Chemical engineering Science

44) H. Witzmann. Z. Elecktrochem, 46, 1940, 313

45) K.R. Duggirala, J.C. Roy, M.S. Saeidi, M.J. Khodadadi, R.D. Cahela and J.B. Tatarchuk, Pressure drop prediction in micro-fibrous materials using computational fluid dynamics, ASME Journal of Fluid Engineering (130) (2008), pp. 071302-1–071302-13

46) S.A. Hosseini and H.V. Tafreshi, 3-D simulation of particle filtration in electrospun nanofibrous filters, Powder Technology 201 (2010), pp. 153–160

47) E. Schweers and F. Löffler, Realistic modeling of the behaviour of fibrous filters through consideration of filter structure,Powder Technology 80 (1994), pp. 191–206

48) J. Ohser and F. Mücklich, Statistical Analysis of Microstructures in Materials Science, Wiley, Chichester (2000)

49) D.O. Banks, Stokes flow through a system of parallel infinite cylinders with axes oriented at angle top the direction of mean flow, Particulate Science and Technology 5 (1987), pp. 339–353

50) Banks, D.O., Kurowski, G.J., Whitaker, S., 1990. Diffusion deposition on a fiber in non-transverse flow. In: Proceedings of the Second World congress: Particle Technology

51) E. Schweers and F. Löffler, Realistic modeling of the behaviour of fibrous filters through consideration of filter structure, Powder Technology 80 (1994), pp. 191–206.

52) Tafreshi HV, Fotovati S, Pourdeyhimi B, Influence of fiber orientation distribution on performance of aerosol filtration media, Chemical Engineering Science, 65(18), 2010, pp 5285–5293

53) M.A. Tahir and H.V. Tafreshi, Influence of fiber orientation on the transverse permeability of fibrous media, Physics of Fluids 21(2009), p. 083604

54) O. Lastow and A. Podgorski, Single-Fiber Collection Efficiency. In: K.R. Spurny, Editor, Advances in Aerosol Filtration, Lewis Publisher, CRC Press LLC (1998)

55) S. Kuwabara, The forces experienced by randomly distributed parallel circular cylinders of spheres in a viscous flow at small Reynolds number, Journal of the Physical Society of Japan 14 (4) (1959), pp. 527–532

56) Hinds W, Aerosol technology, second edition, Wiley & Sons, 1998

57) Kirsch, Stenchkina. A contribution to the theory of fibrous aerosol filters. Faraday Symposium of the Chemical Society, 7, 143, 1973

58) C.N. Davis, I.B. Stechkina, A.A. Kirsch and N.A. Fuchs, Studies on fibrous aerosol filters—IV. Calculus of aerosol deposition in model filters in the region of maximum penetration, Annals of Occupational Hygiene 12 (1969), pp. 1–8

59) J. Pich, In aerosol science, Academic Press, New York (1966)

60) J. Pich, The filtration theory of highly dispersed aerosols, Staub Reinhalt Luft 5 (1965), pp. 16–23 in English

61) J. Pich, Pressure drop of fibrous filters at small Knudsen numbers, Annals of Occupational Hygiene 9 (1966), pp. 23–27

62) S. Jaganathan, H.V. Tafreshi and B. Pourdeyhimi, On the pressure drop prediction of filter media with bimodal fiber diameter, Powder Technology 181 (2008), p. 89

63) O. Lastow and A. Podgorski, Single-Fiber Collection Efficiency. In: K.R. Spurny, Editor, Advances in Aerosol Filtration, Lewis Publisher, CRC Press LLC (1998)

64) Liu, B.Y.H., Rubow, K.L. (1990). Efficiency, pressure drop and figure of merit of high efficiency fibrous and membrane filter media,Fifth world filtration conference, Nice, France

65) H.V. Tafreshi, M.S. Rahman, S. Jaganathan, Q. Wang and B. Pourdeyhimi, Analytical expressions for predicting permeability of bimodal fibrous porous media, Chemical Engineering Science 64 (6) (2009), pp. 1154–1159

66) N. Rao and M. Faghri, Computer modeling of aerosol filtration by fibrous filters, Aerosol Science and Technology 8 (2) (1988), pp. 133–156

67) C.N. Davies, Air Filtration, Academic Press, London (1973)

68) J. Pich, Pressure drop of fibrous filters at small Knudsen numbers, Annals of Occupational Hygiene 9 (1966), pp. 23–27

69) S.A. Hosseini and H.V. Tafreshi, Modeling permeability of 3-D nanofiber media: effects of slip flow, Chemical Engineering Science 65 (2010), p. 2249.

70) S.A. Hosseini and H.V. Tafreshi, 3-D simulation of particle filtration in electrospun nanofibrous filters, Powder Technology 201 (2010), pp. 153–160

71) B. Maze, H.V. Tafreshi, Q. Wang and B. Pourdeyhimi, Unsteady-state simulation of nanoparticle aerosol filtration via nanofiber electrospun filters at reduced pressures, Journal of Aerosol Science 38 (2007), p. 550

72) W.G. Jackson and F.D. James, The permeability of fibrous porous media, *The Canadian* Journal of Chemical Engineering 64(1986), p. 364.

73) R.C. Brown and A. Thorpe, Glass-fiber filters with bimodal fiber size distributions, Power Technology 118 (2001), p. 364-671

CHAPTER 2

EXPERIMENTAL SETUP

This chapter provides information about the various parameters and apparatus used for the study. This includes description of the polymer solution, substrate sample, electrospinning apparatus, corona, filter test rig, imaging and analyzing techniques. The conditions used for each process are also mentioned in brief. Effects of different corona positions and corona voltages are also discussed in the chapter

Nylon 4, 6 polyamide was dissolved in formic acid to prepare 10% and 18 % Nylon 4, 6 polymer solutions by weight. These solutions were electrospun onto Nylon 6 coarse mesh substrate to form non woven filter mats. 10% Nylon 4, 6 solution was used to prepare unimodal mats while 10% and 18% solutions were used to prepare bimodal filters. It was observed that the depositing fibers resulted in positive charge accumulation on the substrate. To neutralize the surface charge on the mats, a corona was added to the original electrospinning setup. The morphology of the filter mats was analyzed using electron microscopy. The filters were tested for

their performance; parameters included were efficiency, pressure drop and Figure of Merit.

2.1 Materials

2.1.1. Polymer solution

Nylons or polyamides are one of the most commonly used polymers to draw fibers. Nylon 4, 6 is a symmetrical linear molecular chain, $(C_{10}H_{22}N_2O_4)_n$ consisting of high content of polyamide. It has a high molecular weight (M = 234.29 g/mol) and a melting point ,T_M = 295 °C. It has a density of ρ = 1.18 g/mL. The molecular symmetry leads to self -nucleation, rapid crystal growth and, thus, a higher level of crystallinity in nylon 4,6. Higher crystallinity leads to properties like higher strength, higher stiffness, high heat-deflection temperature (HDT), high fatigue resistance, high wear resistance, and high creep resistance [1].

Formic acid is the simplest carboxylic acid abundantly found in nature. It is a colorless fuming liquid with a pungent odour with properties are M= 46.03 g/mol, T_M = 8.4 °C, T_B = 100.7 °C , ρ = 1.6 g/mL. It is highly miscible with water. The characteristics of formic acid are its failure to form an anhydride and its reactivity as a reducing agent [1] .

Sigma-Aldrich nylon 4,6 (442992; CAS=50327-22-5) dissolved in Formic acid (98%, Fluka 06440) was used in the study. Electrospinning of thinner jets often leads to bead formation in the fibers [2]. To increase the net charge density and thus the ionic conductivity for smoother fiber formation, 0.4 weight % pyridine (99%, Sigma-Aldrich 360570) was added to the solution.

The polymer solution was prepared in 10 mL vials. It took two days for the polymer to dissolve completely in the solvent. The solution was then refrigerated and used for a period of one month before being discarded.

2.1.2 Substrate sample

The substrate used was Nylon 6 coarse square mesh, N-30. Previous study showed that the formic acid not evaporated during the spinning process would dissolve the nylon substrate [4]. The wet fibers would adhere strongly to any material soluble in formic acid. This created a strongly bonded filter mat. Use of nylon 6 substrate was continued for this study. The samples for the study consisted of the substrate cut into circles of approximately 1.2 cm^2 area over which nylon 4, 6 fibers were spun. The weight of the substrate samples was in the range of 14-16 mg. The mesh had a thickness of 0.273 mm and an open area of 36.8 %.

2.2 Electrospinning apparatus

The electro spinning apparatus consisted of a high voltage D.C. source, an infusion pump, a corona (negative ion source for neutralizing surface charge) and a rotating aluminum cylindrical drum. Substrate samples were mounted using two small pieces of copper tape (typically 2 x 4 mm) onto a grounded aluminum drum which acted as a collector. This hexagonal cylindrical drum is 6.5 inches long, the spacing between parallel faces is 1 inch and each face width is 0.55 inches. The drum was mounted to a lathe (Micro lathe II, Model 4500), and was rotated at 1200 rpm via belt connection to an AC motor (Marathon Electric, Cat No. S102). An electrospinning needle assembly and a corona assembly were positioned on either side of the drum axis. The electrospinning needle assembly consisted of a flat tip stainless steel (SS) 23G needle (Becton-Dickinson, PrecisionGlide^{TM}) of length ½". It was connected to a 1 cc plastic syringe (National Scientific Company, #S7510-1) containing the polymer melt solution. This solution syringe was placed in an infusion pump (Harvard Apparatus PHD2000). The flow rate was set to 0.6 μL/min. The distance between the needle tip and the drum axis was 10 cm. A voltage of 7.5 kV was applied to the needle by a Matsusada Precision Inc. power supply (Model AMT-10810-LCS). The corona was placed 4.5 mm from drum surface, its tip coaxial to the needle tip. A

negative voltage of 3.5 kV was given to the corona with Spellman power supply (model CZE1000R). The collector drum was electrically grounded. It was also ensured that all other electrical devices were properly grounded at one end. All voltage and current measurements were taken either directly from the power supplies or using an Agilent 34401A digital multimeter and/or a Fluke 80k-40 HV probe. Temperature and humidity measurements were taken before each experiment using a Vaisala HM 34 meter. Figure 2.1 schematically outlines the electrospinning apparatus setup.

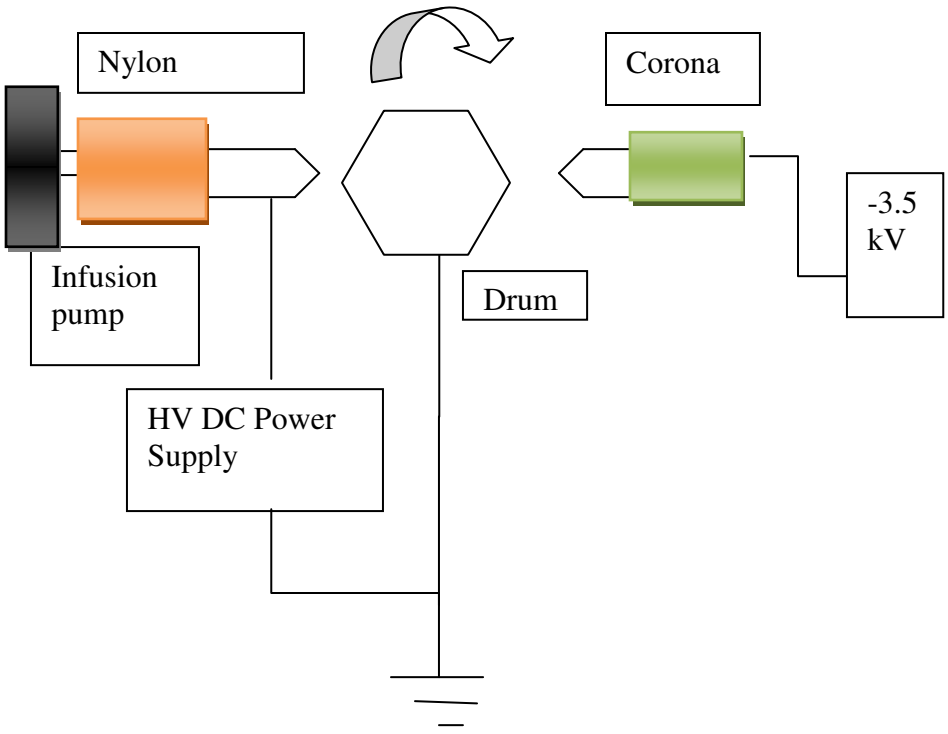

Figure 2.1 Electrospinning apparatus setup

2.3 Filter Test Rig

The filter test rig (FTR) arrangement with rotameter, optical particle counter (OPC) and pressure meter is shown in figure 2.2. The FTR was attached to a Brooks's tube 1110 and 1140 series flowmeter (R-2-15-B). This rotameter has a maximum flow of 4.4 LPM at 14.7 psia and 70 °F. Since the optical particle counter attached to the end of FTR is fixed at a volumetric flow rate of 2.8 LPM, the actual flow rate and hence velocity of air passing through the filter was controlled at desired conditions by fixing the rotameter flow. A HEPA filter is attached to the tube connecting the rotameter and test rig. This ensures that the particle counts given by the OPC are solely for the filter in the test rig.The pressure meter is connected to the two ports of the test rig. Pressure reading are taken directly from the digital pressure meter.

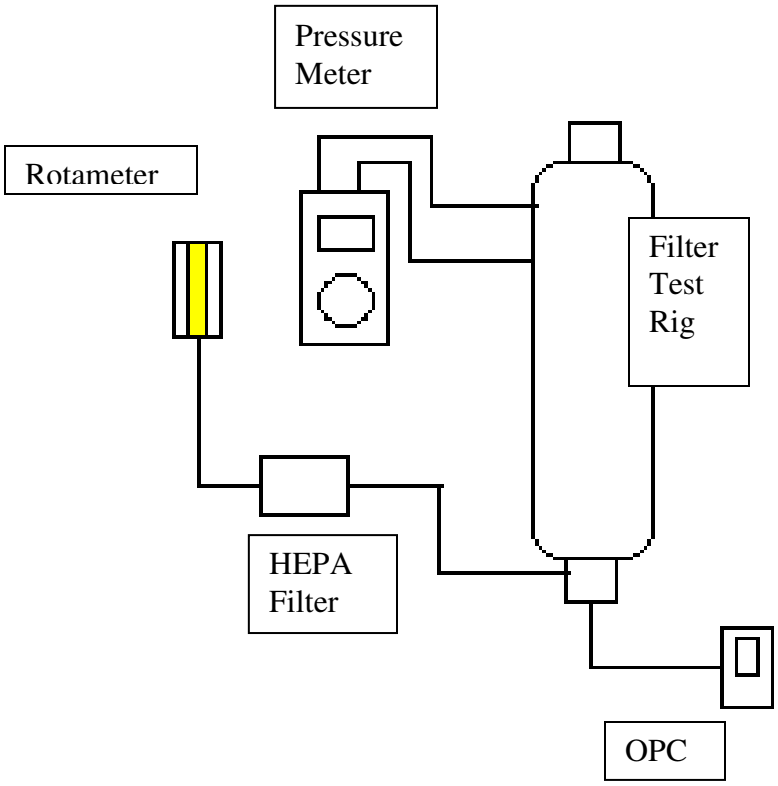

Figure 2.2: Pressure measurement Test Rig Set up

The filter test rig, shown in Figure 2.3, is like a vertical orificemeter with the pressure ports in the upper and lower pieces. The two ports measure the pressure upstream and downstream of the flow and are connected by Tygona tubing (1/8" ID, ½" OD) to the digital pressure meter.

The upper piece is 40 mm long with a center tapped bore of 9.4 mm diameter. It also has a conical inlet, 1 cm long with top and bottom diameters of 22.0 and 9.4 mm respectively allowing air to enter the FTR through a 1 cm long conical opening, having a 30°

edge. The pressure port is of wire gauge size 76 and is placed between the inner bore and outer surface at 38 mm from top .

The lower piece also has a 9.4 mm center tapped bore running the entire length. The lower piece is 50 mm in length, 12.6 mm diameter with conical opening at the lower end. (32 mm long, top and bottom diameters 11 mm and 3 mm respectively). A pressure port of the same size as in upper piece is placed 80 mm from the bottom. The inlet piece allows airflow into the optical particle counter (OPC) and is connected with rubber tubing (supplied with OPC, 9 mm OD, 6 mm ID).

The inlet and lower piece are fitted together coaxially. The filter is placed between the upper and lower piece. An O-ring is placed on either side of the piece with the filter resting in between the O-rings. The O-rings give the necessary compressive force to the filter thus making sure that all air is forced through it.

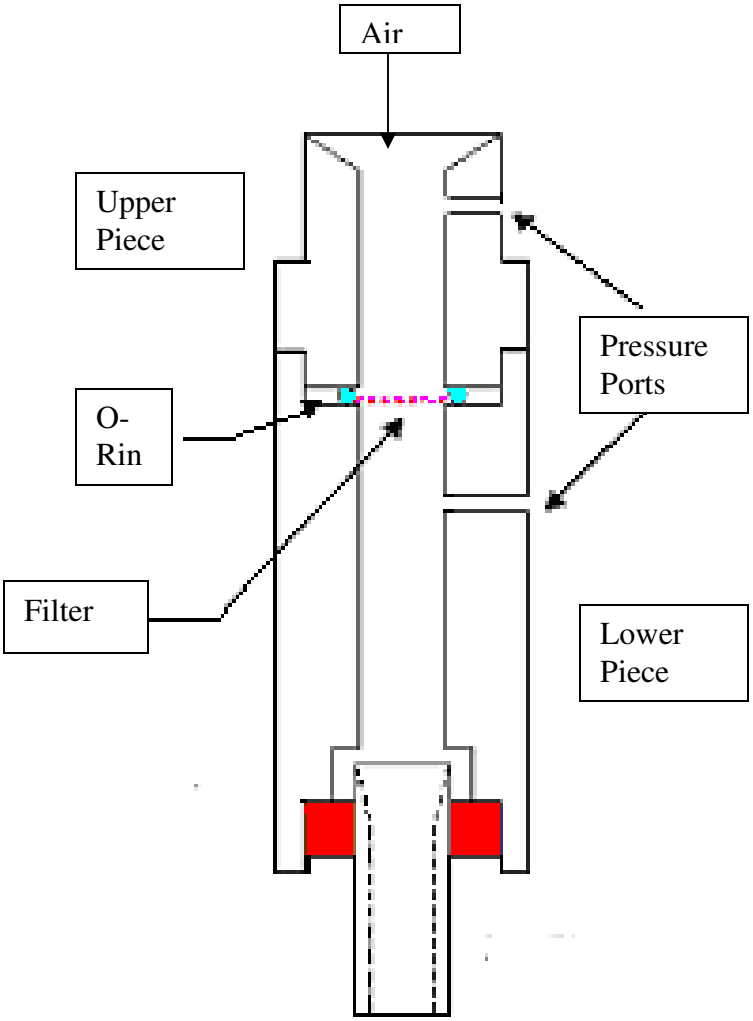

Figure 2.3: Filter Test Rig

2.4 Optical Particle Counter (OPC)

An AeroTrak™ Handheld Optical Particle Counter (OPC), Model 8220 was used for all filtration efficiency measurements. The flow rate is fixed at 2.8 LPM. This flow rate was verified using the rotameter setup described above. The OPC has a particle size range of 0.3 to 10 µm. It has six user definable bin sizes with 0.01 µm

increments. Measurements were taken with 0.3, 0.4, 0.7, 1.0 and 2.0 μm bin cutoffs for 2 minute duration. Measurements for 0.3 - 0.4 bin were considered in performance evaluation.

2.5 Scanning Electron Microscopy (SEM)

The morphology of the fiber mats was analyzed using a Hitachi Scanning Electron Microscopes. The parameters for microscopy included beam voltage of 3-5 kV, working distance of 6 mm, detector bias of +400 V and column aperture of 30 mm. The samples were mounted to stainless steel sample holders of 0.5 inch diameter using carbon adhesive tape. Since the samples were non-conductive, they were coated with carbon paint to add conductivity .Samples were then sputter coated in platinum for 20 minutes. Due to the extra conductivity of carbon paint, comparatively clearer imaging was obtained.

2.6 Optical Microscopy

An OPELCO model Olympus BX60 microscope was used for all optical imaging. Images were taken at 5X, 10X, 20X and 50 X magnifications with top lighting. An Infinity 1-3C CCD camera was used to capture all images.

2.7 Weighing Scale

An Ohaus Discovery DV 114 C precision high lab balance was used to measure the mass of the deposited fibers. The capacity and readability was 110 g and 0.1 mg. The repeatability was 0.003 g. Since the substrate acted as a support base to deposited fibers and did not contribute to particle collection and also had no resistance to air flow, the fiber mats themselves were the actual filters. Each substrate was initially weighed before being used for electrospinning deposition. The acceptable range was 14-16 mg. After the fibers were deposited, these mats were then again weighed. The difference between the two weights gave the mass of the deposited fibers to an accuracy of ±0.01 mg.

2.8 Data Analysis Methods

The pressure drop for the filter, Δp, was calculated by taking the difference between upstream and downstream pressure readings. This pressure drop was displayed directly on the pressure meter (Extech HD 700 differential manometer, 09072984) in units of inches of mercury. This was converted into Pascal. The penetration through the filter, P was calculated by taking the ratio of background particle counts (no filter) and filtered particle counts.

Filtration efficiency is equal to 1- penetration, where the penetration P is defined as

$$P = \frac{\text{particle concentration downstream of the filter}}{\text{particle concentration upstream of the filter}}$$

The filter performance was calculated in terms of Figure of Merit (FOM). FOM or Quality Factor if defined as $Q = \frac{-\ln(P)}{\Delta p}$.

All graphs and calculations were done in MS Excel 2003 and 2007.

2.9 Neutralization of Surface Charge

The electrospun fibers on the substrate carry some amount of positive charge. If the rate of charge deposition is higher than the rate of charge dissipation charge accumulation will occur. With a dielectric substrate, a critical saturation point is reached where no further deposition occurs because of the electrostatic repulsion between the fibers and the substrate. To neutralize this surface charge on the substrate, a negative charged corona was used. A corona is created when a high voltage is placed on a sharp point. In the study, a negative potential was given to the corona. This caused the corona to create negatively charged ions. These ions were deposited onto the collector drum and the substrate. Hence the

positively charged ions from fibers were neutralized due to negatively charged corona ions.

2.10 Effect of corona voltage on fiber mat

The applied voltage to the needle tip was + 7.5 kV. The corona was placed 4 mm from the collector drum. A potential of – 4.5 kV was given to the corona. The mat surface showed small holes on visible observation. On observing under an electron microscope it was found that the fiber deposition on the surface had random large gaps which resulted in less aerosol retention. These holes or gaps were created by the high corona voltage due to an electric breakdown in an effect similar to lightning. To eliminate these holes, the corona voltage was reduced to -3.5 kV maintaining the same distance as earlier. The new voltage showed no holes on the surface when viewed under an optical microscope. It was also found that the efficiency of the filters was increased on elimination of the holes from the mat surface.

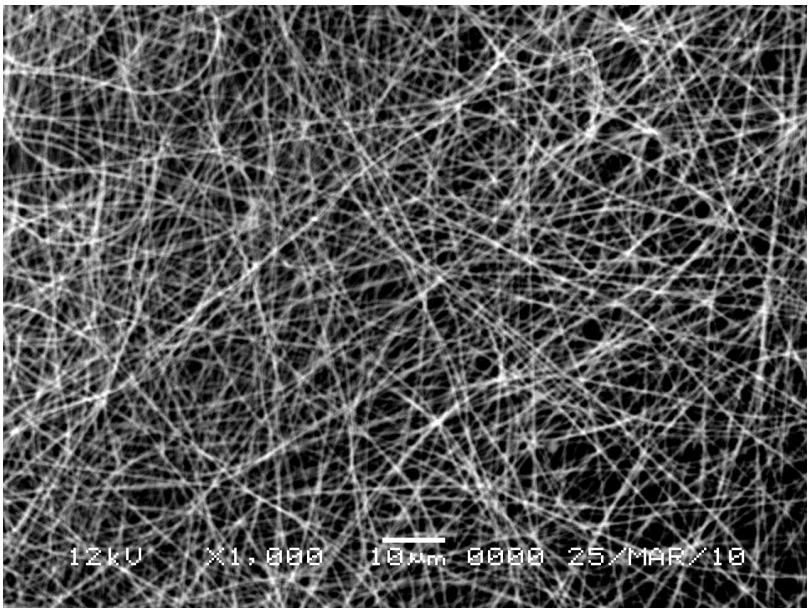

Figure 2.4 Electric breakdown created holes (right bottom)

Uecker et.al had observed that the fiber diameter decreases with the increase in corona voltage [3]. The same was observed in this study. With the corona voltage of -4.5 kV, the fiber diameter was found to be 80±5 nm. On reducing the corona voltage to -3.5 kV, the fiber diameter increased to 100±8 nm. As the fiber diameters are below 500 nm, the fiber mats would still observe a slip effect.

2.11 Bimodal Deposition

The bimodal mats were to have approximately equal mass (± 0.01 mg) as that of unimodal mats. Two modes of deposition were considered for the bimodal filters- sequential deposition and simultaneous deposition.

In sequential deposition, the filter consisted of alternate layers of 10% and 18%. Each layer was spun for the same period; i.e. the

total spinning time and the resultant number of layers were same for both 10% and 18%. Simultaneous deposition consisted of spinning of 10% and 18% solution concentrations at the same time. The time required for simultaneous mode of deposition was half compared to sequential deposition mode. It was observed that the pressure drop for mats of both modes was similar. However, the sequential deposition mode mat showed consistently slightly higher efficiency than the simultaneous mats shown in table 2.1.

Table 2.1 Performance of simultaneous and sequential bimodal mats

Sample	Efficiency	Pressure Drop	FOM
Seq 1	98.2	390	0.011
Seq 2	99.1	396	0.0112
Seq 3	98.8	389	0.0101
Seq 4	99.3	400	0.011
Seq 5	98.89	398	0.01
Sim 1	98	386	0.011
Sim 2	98.2	388	0.0102
Sim 3	97.95	380	0.01
Sim 4	98.75	392	0.0102
Sim 5	98.63	390	0.01

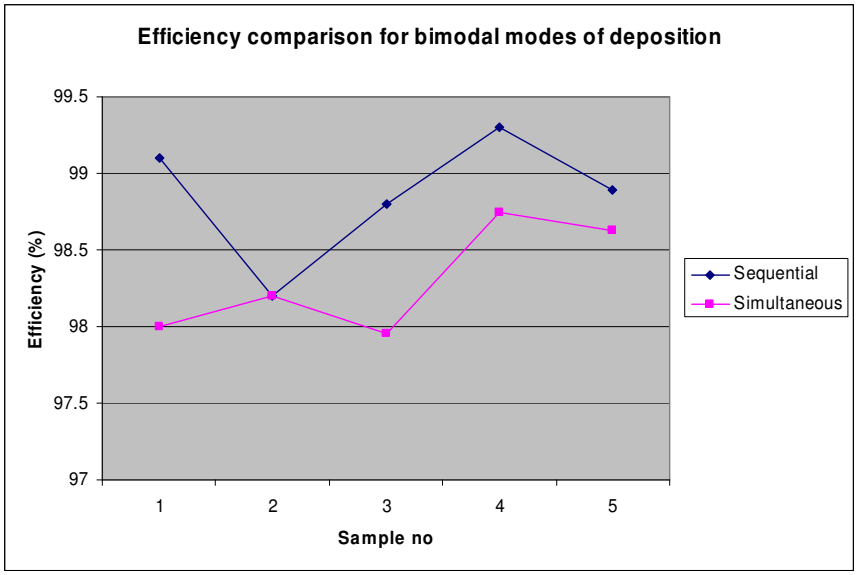

Fig. 2.5 Chart depicting efficiency comparison

As the study targeted preparation of HEPA filters, the simultaneous deposition mode was discarded in favor of sequential, layered bimodal mats.

List of References

1] The Merck Index, Merck Publishing Company, New Jersey, Oct. 2006, Edition 14

2] H. Fong, I. Chun, D. Renekar, Beaded nanofibers formed during electrospinning, Polymer 40 (1999) 4585–4592

3] Uecker J, Tepper G.C, Rosell-Llompart J, Ion- assisted collection of Nylon 4,6 electrospun nanofibers, Polymer 51 (2010) 5221-5228

4] Uecker J.C, The production and filtration efficiency testing of nonwoven electrospun mats, Thesis for Masters of Science, 2007.

CHAPTER 3

RESULTS AND DISCUSSION

3.1. Unimodal filter mats

Nylon 4, 6 solution in formic acid was prepared for 10% weight concentration. Using the process parameters as described in chapter 2, the solution was electrospun onto the substrate. For fiber deposition of 0.33 mg, the spinning time was 210 minutes. The filters were tested in the filter test rig as described in Chapter 3. The face velocity across the filter was 5 cm per second. Penetration calculations were taken without the filter and then with the filter. The ratio of the two gave the penetration for the filter. Figure of Merit or Quality factor was calculated as described in Chapter 1. Table 3.1 shows the evaluation data for the 0.33±0.01 mg unimodal filters:

Table. 3. 1. Table of performance for unimodal filters of 0.33±0.01 mg

Sr. No	Pressure (in. Hg)	Pressure (Pa)	Efficiency	FOM
1	0.334	1127.25	0.994	0.004
2	0.321	1083.38	0.994	0.005
3	0.319	1076.63	0.993	0.005
4	0.329	1110.38	0.993	0.004
5	0.323	1090.13	0.995	0.005
Average	**0.325**	**1097.55**	**0.994**	**0.005**

For fiber deposition of 0.66 ±0.01 mg, the nylon 4, 6 10% solution was spun for 420 minutes continuously. Table 2 depicts the data for the same:

Fig 3.2 Table of performance for unimodal filters of 0.66 mg

Sr. No	Pressure (in. Hg)	Pressure (Pa)	Efficiency	FOM
1	0.634	2139.75	0.997	0.003
2	0.645	2176.88	0.996	0.002
3	0.657	2217.38	0.997	0.003
4	0.663	2237.63	0.998	0.003
5	0.639	2156.63	0.996	0.003
Average	**0.648**	**2185.65**	**0.997**	**0.003**

3.2 Bimodal filter mats

The bimodal filter mats were a layered composite of thick and thin fibers. Thin fibers were produced by spinning 10% nylon 4, 6 solution concentration while the thick or coarse fibers were obtained by spinning 18% 4, 6 nylon solution concentration. The bimodal mats were designed to have approximately equal total mass as that of unimodal mats. The mass fraction of thick and thin fibers was 0.6 and 0.4 respectively.For filter mass of 0.33 mg, the 10% polymer solution had to be spun for 72 minutes and the 18% solution concentration to be spun for 60 minutes at the infusion rate of 0.6 microlitres per minute. The 10% and 18% solution were alternately spun. Thus the bimodal mats were layered mats with each layer alternating between individual fine and coarse fiber mats. The process and testing parameters were kept the same. Table 3.3 gives the data for 0.33±0.01 mg bimodal mats. For fiber deposition of 0.66 ±0.01 mg in bimodal mats, 10% solution was spun for 144 minutes while the 18% solution was spun for 120 minutes. Table 3.4 gives the data evaluated for the same.

Sr. No	Pressure (in. Hg)	Pressure (Pa)	Efficiency	FOM
1	0.102	344.25	0.982	0.012
2	0.107	361.13	0.987	0.012
3	0.101	340.88	0.982	0.012
4	0.1	337.50	0.981	0.012
5	0.108	364.50	0.990	0.013
Average	**0.104**	**349.65**	**0.984**	**0.012**

Table 3.3 Performance of bimodal filters of 0.33±0.01 mg

Fig 3.4 Table of performance for bimodal filters of 0.66 ±0.01 mg

Sr. No	Pressure (in. Hg)	Pressure (Pa)	Efficiency	FOM
1	0.204	688.50	0.991	0.007
2	0.217	732.38	0.989	0.006
3	0.206	695.25	0.992	0.007
4	0.211	712.13	0.991	0.007
5	0.225	759.38	0.991	0.006
Average	**0.213**	**717.52**	**0.991**	**0.007**

3.3 Filter Mat Morphology

3.3.1 Fiber Diameter

The fiber diameter depended on the solution concentration. It was observed that the fiber diameter was proportional to the solution

concentration. As discussed in the previous chapter the fiber diameter decreased with increasing corona voltage. The fiber diameter values were estimated from analyzing a number of filters with SEM. It was observed that the fiber diameters for each solution concentration were not uniform but instead were in a range. It was found that for a negative corona voltage of 3.5 kV, the 10% solution concentration gave fiber diameters in the range of 100±8 nm while the 18% solution concentration had an average fiber diameter of 190±12 nm. Figure 3.1 gives a distribution of filter diameters for 10% and 18% nylon 4, 6 solution concentrations. Figures 3.2 and 3.3 shows the SEM images for unimodal and bimodal fiber mats.

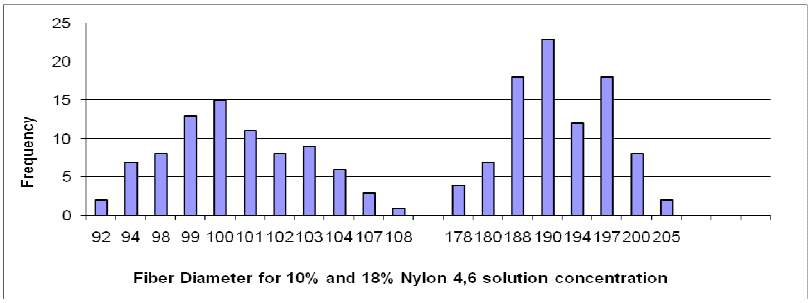

Figure.3.1. Histogram depicting the fiber diameter distribution

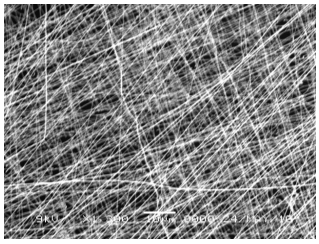

Fig 3.2 SEM Image:

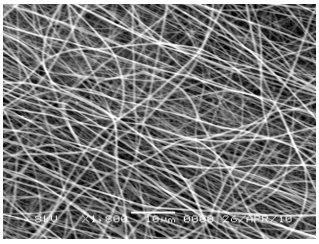

Fig. 3.3 SEM Image

Unimodal fiber mats Bimodal fiber mats

3.3.2 Thickness

The nylon 6 coarse mesh substrate had an average thickness of 273 micrometers. The thickness of the fiber mats was measured using precision calipers. These calipers had the resolution of 1 micron. Table 3.5 gives the thickness distribution for both the unimodal and the bimodal filter mats.

Table 3.5.Thickness distribution of fiber mats

Thickness of fiber mats (microns)		
Fiber weight	Unimodal	Bimodal
0.33 mg	26± 5	20± 3
0.66 mg	52± 4	40± 2

3.4 Comparison of Performance for Unimodal and bimodal filter mats

The unimodal and bimodal filters mats had approximately the same mass. Each filter had an area of approximately 1.18 cm^2. Basis weight was calculated by dividing fiber weight by area. The performance of the two deposition modes was then compared for each basis weight. The results are charted below in figure 3.4:

3.4.1 Pressure Drop

It was observed that the pressure drop increase was proportional to the increase in basis weight for each deposition mode. The unimodal mats had an average pressure drop of 1200 Pa and 2400 Pa for basis weights of 0.0028 and 0.0056 respectively. For these, the bimodal mats showed significantly lower pressure drop of 350 Pa and 700 Pa average.

3.4.2 Efficiency

The unimodal mats showed high efficiencies, with efficiencies > 99% for each basis weight. However, the efficiency did not significantly increase with increasing basis weight. The average efficiency for basis weight of 0.0028 was 99.3% while that for 0.0056 was 99.6%. The bimodal mats showed lower efficiencies compared to unimodal mats. However, the efficiency increase was better compared to unimodal. The average efficiency of 0.33 mg bimodal mat was 98.4 % while 0.66 % showed efficiencies of 99.1%

3.4.3 Figure of Merit (FOM)

The figure of Merit was calculated as given from chapter 1. It was seen that the unimodal mats had FOM a magnitude lower than

required by HEPA standards. The bimodal mats however had FOM very close to required 0.03 HEPA [5].

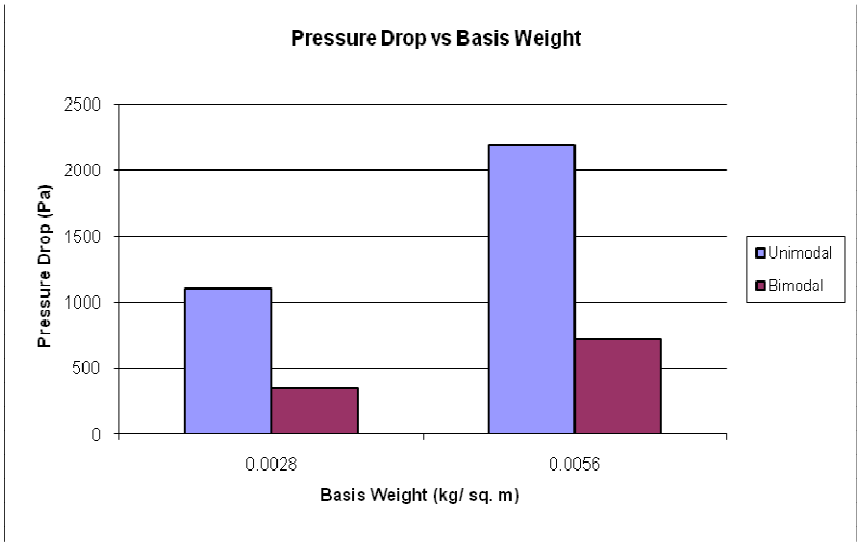

Fig 3.4. Chart comparison between unimodal and bimodal filters for pressure drop

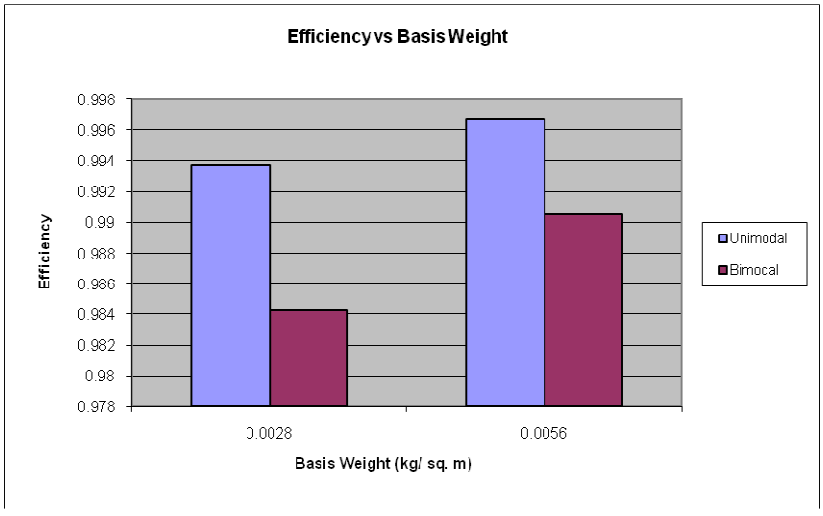

Fig. 3.5. Chart Comparison between unimodal and bimodal filters for Efficiency

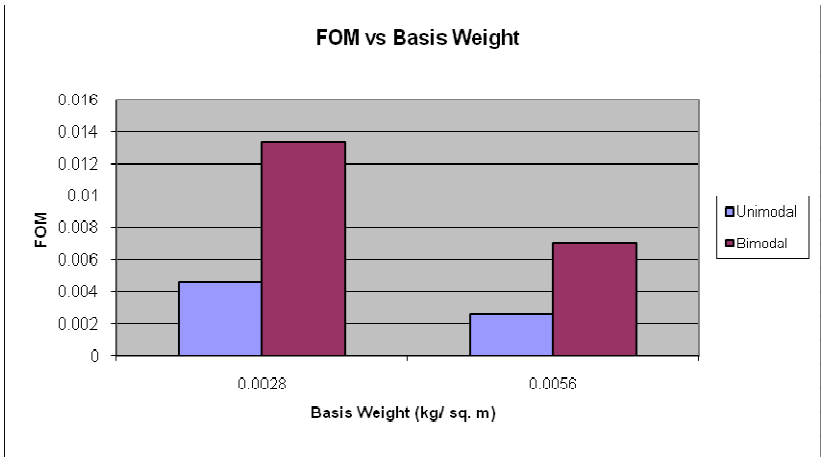

Fig. 3.6. Chart comparison between unimodal and bimodal filters for Figure of Merit

3.5 Theoretical Calculations

Using the calculations as given in Chapter 1, the various parameters for performance were evaluated.

3.5.1 Solidity (α) [1]

The solid volume fraction for unimodal and bimodal filters was calculated and is given in the table 3.6 .

Table 3.6: Solid volume fraction

SVF (α) (%)		
Fiber weight	Unimodal	Bimodal
0.33 mg	9.126	11.864
0.66 mg	9.126	11.864

3.5.2 Dimensionless pressure drop f(α) [1–3]

Davies Equation gives the formula for f(α)

$$f(\alpha) = 64\alpha^{3/2} * (1 + 56 * \alpha^3) \quad \ldots\ldots\ldots\ldots(1)$$

Incorporating the Tafreshi-Hosseini correction factor, f(α) is calculated for both deposition modes. It is approximately 0.67.

$$f(\alpha) = 0.67 * 64 * \alpha^{1.5} * (1 + 56 * \alpha^3) \quad \ldots\ldots(2)$$

Using this parameter, the resistance to air flow for a filter of given solid volume fraction and thickness can be calculated mathematically. The dimensionless parameter f(α) was 1.17 and 1.62 for unimodal and bimodal filter mats respectively.

3.5.3 Pressure Drop Calculations[1–3]

The pressure drop across unimodal filter is given by

$$\Delta p = f(\alpha)\frac{\mu t V}{d^2{}_f} \quad \ldots\ldots\ldots\ldots\ldots\ldots(3)$$

Where μ: viscosity of air = 1.78 x 10^{-5}

T: fiber mat thickness

V: face velocity= 5 cm/sec

d_f: fiber diameter= 100 nm

For bimodal filters, the fiber diameter is the equivalent fiber diameter of fine and coarse fibers.The equivalent fiber diameter is given by the cube root equation of Tafreshi

$$d^{cr}_{eq} = 2 * \sqrt[3]{n_c r_c^{\,3} + n_f r_f^{\,3}} \quad \text{.....(4)}$$

n_c, n_f, r_c, r_f are the number fractions and radii of coarse and fine fibers respectively.

Substituting the equivalent diameter in the pressure drop equation, the resistance to air flow for bimodal filter mats can be calculated.

The calculated and experimental pressure drop values for unimodal and bimodal mats are given in the table 3.7

Table 3.7 Pressure drop values for unimodal and bimodal filters calculated from theoretical equations

Pressure Drop (Δp) (Pa)				
	Calculated		Experimental	
Fiber weight	Unimodal	Bimodal	Unimodal	Bimodal
0.0028 kgm^{-2}	2707	1046	1200	350
0.0056 kgm^{-2}	5414	2092	2400	700

3.5.4 Efficiency Calculations [3–4]

The efficiency of a filter is given by the equation

$$\eta = 1 - \exp\left[-\frac{4\alpha E t}{\Pi(1-\alpha) d_f} \right] \quad \text{.....(5)}$$

$$E = 1 - (1 - E_D)(1 - E_R)(1 - E_I) \quad \text{.....(6)}$$

E_D, E_R and E_I are the single fiber efficiencies due to diffusion, interception and inertial impaction respectively

The calculated and experimental efficiencies are given in table 3.8

Table 3.8 Calculated efficiency values for unimodal and bimodal filters

Efficiency (%)				
	Calculated		Experimental	
Basis weight	Unimodal	Bimodal	Unimodal	Bimodal
0.0028 kgm^{-2}	99.9999	99.9999	99.3	98.4
0.0056 kgm^{-2}	99.9999	99.9999	99.6	99.1

3.5.5 Quality Factor Or Figure of Merit [4–7]

The Figure of Merit (FOM) is given by $Q = \frac{-\ln(P)}{\Delta p}$

The theoretical and experimental FOM are calculated and are given in table 3.9:

Table 3.9. Calculated FOM values for unimodal and bimodal filters

FOM				
	Calculated		Experimental	
Basis weight	Unimodal	Bimodal	Unimodal	Bimodal
0.0028 kgm^{-2}	0.0033	0.0088	0.0044	0.013
0.0056 kgm^{-2}	0.002	0.0044	0.003	0.007

List of References

1] J. Pich, In aerosol science, Academic Press, New York (1966)

2] S.A. Hosseini and H.V. Tafreshi, Modeling permeability of 3-D nanofiber media: effects of slip flow, *Chemical Engineering Science* 65 (2010), p. 2249

3] Fotovati S, Tafreshi HV, Pourdeyhimi B, Influence of fiber orientation distribution on performance of aerosol filtration media, CES, 65(18), 2010, pp 5285–5293

4] Liu, B.Y.H., Rubow, K.L. (1990). Efficiency, pressure drop and figure of merit of high efficiency fibrous and membrane filter media,*Fifth world filtration conference*, Nice, France

5] D. Sinclair, Penetration of HEPA filters by submicron aerosols, *Journal of Aerosol Science* 1 (1970), pp. 53–67

CHAPTER 4

CONCLUSION

Nylon 4, 6 solution in formic acid was prepared for weight concentrations of 10% and 18%. Unimodal filter mats of fine fibers were prepared by spinning 10% Nylon 4,6 solution on the substrate. For approximately equal mass, bimodal mats were prepared by laying composite layers of alternate 10% solution and 18% solution. The substrate acted as support for the deposited fibers and had a pressure drop 0.0001 Pa. The substrate did not contribute to the efficiency of the filter. The performance of approximately equal mass unimodal mats and bimodal mats was compared. It was observed that while bimodal mats had lower efficiencies and pressure drop compared to unimodal mats, the FOM was almost 200% higher. For a given filter of known basis weight and thickness, its solidity, pressure drop, efficiency and FOM can be calculated. The theoretical calculations qualitatively matched the experimental observations. The discrepancies in the theoretical pressure drop could be accounted for non-

uniformity and error in thickness measurement. The theoretical formulae for single fiber efficiency had limitations due the ratio of particle diameter to fiber diameter giving an overestimated calculated efficiency. The FOM does not depend on thickness and showed the same qualitative trend as observed experimentally. From this study, it can be sufficiently concluded that due to high performance of layered composite bimodal mats, they could be considered for future research on HEPA and ULPA filters.